IEEE Access
Multidisciplinary ⋮ Rapid Review ⋮ Open Access Journal

Received 27 March 2024, accepted 15 April 2024, date of publication 18 April 2024, date of current version 29 April 2024.

Digital Object Identifier 10.1109/ACCESS.2024.3390682

RESEARCH ARTICLE

A New Micro-Subcarrier OFDM-Based Waveform for Delay Doppler Domain Communication

SWAROOP GOPALAM[1], (Member, IEEE), SIBIRAJ B. PILLAI[2], PHILIP WHITING[1], HAZER INALTEKIN[1], (Member, IEEE), IAIN B. COLLINGS[1], (Fellow, IEEE), AND STEPHEN V. HANLY[1], (Fellow, IEEE)

[1]School of Engineering, Macquarie University, Sydney, NSW 2109, Australia
[2]Department of Electrical Engineering, IIT Bombay, Mumbai 400076, India

Corresponding author: Swaroop Gopalam (swaroop.gopalam@mq.edu.au)

This work was supported by Australian Research Council's Discovery Project Funding Scheme under Project DP230102252.

ABSTRACT This paper presents a new OFDM based modulation scheme for communication in doubly dispersive channels. We call this Delay-Doppler OFDM (DD-OFDM). Our waveform has the same sparse-channel benefits as orthogonal-time-frequency-space (OTFS) modulation, while offering advantages in terms of simpler channel estimation, lower symbol error rate and lower out-of-band (OOB) emissions. We propose the DD-OFDM modulation scheme by introducing precoding across frames of frequency subcarriers. We show that the resulting waveform has different data carrying basis functions compared to OTFS modulation. We present the DD-OFDM receiver and derive the base-band model equations. We show that the base-band model for DD-OFDM leads to a simple and accurate channel estimation algorithm in non-integer fractional Doppler channels.

INDEX TERMS Delay-Doppler domain, OTFS, OFDM, Delay-Doppler-OFDM, Micro-subcarrier OFDM.

I. INTRODUCTION

Delay-Doppler (DD) domain modulation is a communication approach for doubly dispersive channels that is robust to Doppler spread and delay spread simultaneously [1]. Time-varying wireless multipath channels have a sparse representation in the DD domain. This has recently been exploited by Orthogonal Time Frequency Space (OTFS) modulation which modulates data symbols using basis functions in the DD domain [1], [2], [3], [4], [5], [6]. OTFS has advantages compared to traditional orthogonal frequency division multiplexing (OFDM) which suffers from inter-carrier interference (ICI) in doubly dispersive channels [1], [2], [3], but there are significant channel estimation challenges for OTFS.

In this paper, we present a new OFDM based DD domain waveform, which we call DD-OFDM. It has the same robustness to Doppler spread as OTFS. We show that DD-OFDM has more accurate and simpler channel estimation, and a superior symbol error rate performance compared to OTFS. DD-OFDM also has lower out-of-band (OOB) emissions.

Early work on communication over the doubly dispersive channel took a time-frequency signalling approach [7], [8], [9]. In time-frequency signalling, data symbols are modulated using time-frequency shifted versions of a *prototype* pulse. Standard OFDM can be viewed within this framework, where the prototype pulse is a rectangular waveform at the symbol rate, and the data symbols of each subcarrier can be interpreted as frequency shifted versions of this pulse. The focus of time-frequency signalling was on the design of transmit and receive pulses to overcome inter symbol interference (ISI) and ICI [8], [9], [10]. This is a challenge when channels are fast fading, with high Doppler and delay spread, which cause ICI and ISI respectively, which limits the time-frequency approaches.

OTFS is a DD signalling approach that works directly in the DD domain. The key idea of OTFS is to multiplex information symbols using basis functions that are *nearly* localized in the DD domain [1], [3]. In this domain, there are fewer channel parameters and they vary more slowly, compared to the time-frequency domain. The doubly

The associate editor coordinating the review of this manuscript and approving it for publication was Nurul I. Sarkar.

dispersive channel causes these basis functions to undergo a translation along the delay axis due to the time shift caused by the path delay, and a translation along the Doppler axis due to the frequency shift caused by the path Doppler shift, with an additional multiplicative phase shift term. The resulting baseband input output (I/O) relation for OTFS modulation (with rectangular pulses) is a *twisted convolution* [1], [4], [11]. Although twisted convolution is a complicated relationship, the channel sparsity in the DD domain can be exploited for efficient equalization/detection [4], [5], [12], [13], [14], [15], [16].

OTFS implementations have a standard OFDM front-end that uses wide subcarrier spacings[1] [2], [3], [17], [18]. There are critical challenges in this approach, in terms of channel estimation and equalization. The DD baseband model involves discretizing path delays and Doppler shifts to integer multiples (*i.e.* taps) of a DD grid resolution. The delay resolution is given by the inverse of the bandwidth, whereas the Doppler resolution is the inverse of the DD symbol time. A key difficulty in OTFS equalization is that path Doppler shifts appear as phase rotation terms in the twisted convolution equation. As a result, OTFS requires knowledge of not only DD channel tap gains but also the path Doppler shifts which are real valued. Equalization performance depends on the accuracy of the estimated channel information [5], [19]. In general, there is sufficient resolution along the delay dimension due to the wide bandwidth [5]. However, the Doppler resolution level is limited since the symbol time has to be small, due to latency constraints and a need to stay within the coherence period of the DD domain channel. As a result, non-integer fractional Doppler shifts need to be considered for practical implementations [5], [19], [20], [21], [22].

Several DD channel estimation schemes have been proposed for OTFS over non-integer fractional Doppler channels. In [5], an efficient embedded pilot based channel estimation scheme was introduced, where guard bands were used around the DD domain pilot symbol which enabled channel measurement in the same OTFS symbol. The approach was not applicable to non-integer channels, however a number of related approaches have since been developed based on [5], which address fractional Doppler to an extent, either at a significant increase in complexity or under special assumptions. In [19] and [21] sparse Bayesian learning based models were proposed to estimate the Doppler shifts from the received pilot symbols. In [20] a non-integer channel was approximated by an integer channel by treating each received pilot symbol as an individual path. In [22] the model was simplified by assuming that there is at most one path in a delay bin, and in [23] a time domain interpolation method was proposed.

[1]Standard OFDM requires wide subcarrier spacing to limit the effect of ICI. Unfortunately, wide subcarriers result in having short OFDM symbols in the time domain, which are prone to ISI and require long time-domain cyclic prefixes.

In this paper, we propose a new DD-OFDM modulation approach that avoids the non-integer fractional Doppler estimation problem by employing *micro* OFDM subcarriers (which have much smaller spacing than the Doppler spread) and exploiting the structure of the resulting inter-subcarrier interference to estimate the DD channel. The resulting equalization task includes a phase compensation term that depends on the path delays. This term can be estimated due to the high resolution in the delay dimension of the DD baseband model. Our approach involves multiplexing data in the DD domain by precoding across a large number of closely spaced micro OFDM subcarriers. Our DD-OFDM waveform has a simple precoded OFDM implementation. It offers simpler channel estimation and superior symbol error rate (SER) performance compared to OTFS, and also has much lower out-of-band (OOB) emissions.

The outline of the paper is as follows. In Section II, we introduce the doubly dispersive channel model. In Section III, we present our DD modulation scheme, DD-OFDM, by introducing micro-subcarriers and precoding of the micro-subcarrier symbols. In Section VII, we present the DD-OFDM receiver and derive the baseband I/O relationship for integer Doppler channel, and in Section VII-C, we present the I/O relationship for general non-integer fractional Doppler case. In Section VIII, we present a simple channel estimation scheme for DD-OFDM, utilizing the I/O relationship derived in Section VII-C. In Section IX, we present the DD-OFDM baseband model for a non-integer fractional delay and fractional Doppler channel, and compare the channel estimation accuracy of DD-OFDM and OTFS in such channels using numerical simulation. In Section X, we present symbol-error rate (SER) and spectral efficiency comparisons of OTFS and DD-OFDM. In Section XI, we present our conclusions.

II. DOUBLY DISPERSIVE CHANNEL MODEL

This section presents the channel model, and highlights challenges for standard OFDM modulation when the channel is both delay spread and time-varying.

A. CHANNEL MODEL

We consider the standard channel model with P paths, where for each path $p \in \{0, \ldots, P-1\}$, the parameters h_p, τ_p and ν_p represent the corresponding gain, delay and Doppler shift respectively. The received baseband waveform can be expressed as

$$r(t) = y(t) + z(t), \tag{1}$$

where $z(t)$ is the receiver noise and $y(t)$ is given by

$$y(t) = \sum_{p=0}^{P-1} h_p e^{j2\pi\nu_p t} x(t-\tau_p), \tag{2}$$

where $x(t)$ is the transmitted signal.

The channel is *doubly dispersive* when it is both frequency selective and time varying (*i.e.* time selective). More

specifically, frequency selectivity corresponds to when the delay spread $\max_p \tau_p$ is in the order of (or greater than) the symbol time. Time selectivity corresponds to when the Doppler spread $\nu_{\max} := 2\max_p |\nu_p|$ is in the order of (or greater than) the inverse of symbol time (*i.e.* subcarrier spacing for OFDM based systems).

The *DD domain coherence period* is defined as the time duration over which the parameters h_p, τ_p and ν_p, do not change significantly, and hence can be treated as constants. The DD domain coherence period has been shown to be in the order of tens of milliseconds and typically much larger than the channel coherence time $\frac{1}{2\nu_{\max}}$. For example, channel coherence time is only half a millisecond for a Doppler spread of 1 kHz.

An assumption that the path parameters remain constant over the transmitted symbol time is implicit in all DD domain modulation schemes [1], [2], [3], [4], [5], *i.e.* while the symbol time is greater than the channel coherence time, it must be less than the DD domain coherence period.

B. STANDARD OFDM IN DOUBLY DISPERSIVE CHANNELS

In traditional OFDM, the subcarrier frequencies are separated by $\Delta f = \frac{\beta}{M}$, where β is the total available bandwidth and M is the number of subcarriers. Δf is typically designed to ensure that the OFDM symbol duration including the cyclic prefix (CP), is much smaller than the channel coherence time (*i.e.* $\Delta f \gg \nu_{\max}$), in order to avoid inter-carrier interference (ICI), and allow single tap equalization in the frequency domain. This wide subcarrier approach fails when the Doppler spread is significant, and leads to inter subcarrier interference in doubly dispersive channels. A common variant of OFDM is DFT-precoded OFDM which also uses wide subcarriers [24].

In 3GPP LTE, the downlink uses traditional OFDM with $\Delta f = 15$ kHz which is significantly wider than the Doppler spread of 75 Hz for typical mobility scenarios. The LTE uplink uses Single Carrier Frequency Division Multiple Access (SC-FDMA) which is a form of DFT-precoded OFDM with the same subcarrier spacing [24]. DFT precoding has no effect on the ICI problem that occurs in high Doppler scenarios, *i.e.* in doubly dispersive channels. Hence, both traditional and DFT-precoded OFDM schemes suffer from ICI in doubly dispersive channels.

III. DELAY-DOPPLER OFDM MODULATION

In this section, we present our new DD domain precoded OFDM waveform, which involves employing micro-subcarriers and a new DFT based precoding approach. We call this delay-Doppler OFDM (DD-OFDM).

A. MICRO-SUBCARRIER OFDM

We propose to use an OFDM symbol time that is much *longer* than the channel coherence time. This long-symbol approach corresponds to having *micro-subcarriers*, where the OFDM subcarrier spacing is much smaller than the Doppler spread. This small subcarrier spacing means that our DD-OFDM symbol is matched to the DD domain coherence period, enabling the DD domain channel parameters to be estimated efficiently.

In our Micro-Subcarrier OFDM, we replace each traditional OFDM subcarrier (of width Δf) by a *frequency-frame* of N micro-subcarriers, each separated by $\frac{\Delta f}{N}$. There are M frequency-frames in our proposed Micro-Subcarrier OFDM symbol, hence MN micro-subcarriers. The micro-subcarrier separation $\frac{\Delta f}{N}$ is much smaller than the Doppler spread $\nu_{\max}$. Hence, each DD-OFDM symbol lasts for $\frac{N}{\Delta f} = NT$ seconds, which is much longer than the channel coherence time, but smaller than the DD domain coherence period.

The component of the transmitted symbol corresponding to frequency-frame $m \in \{0, \ldots, M-1\}$ is

$$x^{(m)}(t) = \frac{1}{\sqrt{NT}} \sum_{k=0}^{N-1} \tilde{x}_k^{(m)} e^{j2\pi\,\Delta f\,(m+\frac{k}{N})t},\ t \in \left[-T_{cp}, NT\right)$$

where $\tilde{x}_k^{(m)}$ is the information symbol placed on the k^{th} micro-subcarrier of frequency-frame m, and T_{cp} is the *time domain* cyclic prefix duration. Note that $T_{cp} > \max_p \tau_p$.

The transmitted symbol, corresponding to all M frequency-frames, is

$$x(t) = \frac{\sum_{m=0}^{M-1} x^{(m)}(t)}{\sqrt{M}} = \frac{1}{\sqrt{MNT}} \sum_{s=0}^{MN-1} \tilde{x}_s e^{j2\pi s \frac{\Delta f}{N} t} \tag{3}$$

where $\tilde{x}_{mN+k} \triangleq \tilde{x}_k^{(m)}$. Note that this corresponds to an OFDM transmitter with MN micro-subcarriers with subcarrier spacing $\frac{\Delta f}{N}$.

Note that our micro-subcarrier approach is not a simple case of taking DFT-precoded OFDM and making the subcarrier spacings narrower. It requires a completely different modulation and precoding approach to exploit the structure of the significant ICI that is introduced by the narrow subcarriers. Additionally, it is not possible to simply use single tap equalization in the frequency domain due to ICI. It requires a multi-tap DD domain equalization approach.

In the next subsection, we present our precoding approach for our micro-subcarrier symbols. A block diagram of our overall DD-OFDM modulation scheme is shown in Fig. 1. In Section VII, we will present the input-ouput relationship for DD-OFDM. In Section VIII, we will present a DD domain equalization approach based on the delay-Doppler channel taps that can be obtained by DD domain channel estimation.

B. DD DOMAIN PRECODING

In this subsection, we present our precoding approach for our micro-subcarrier symbols. The approach is a mapping from the delay-Doppler domain into the frequency-frames, in order to create the DD-OFDM symbol. Fig. 2 presents an overview of the precoding.

The data symbols $\hat{x}_k^{(l)}$ fill a $M \times N$ delay-Doppler grid (as shown in the figure), where $k = 0, \ldots, N-1$ are the Doppler

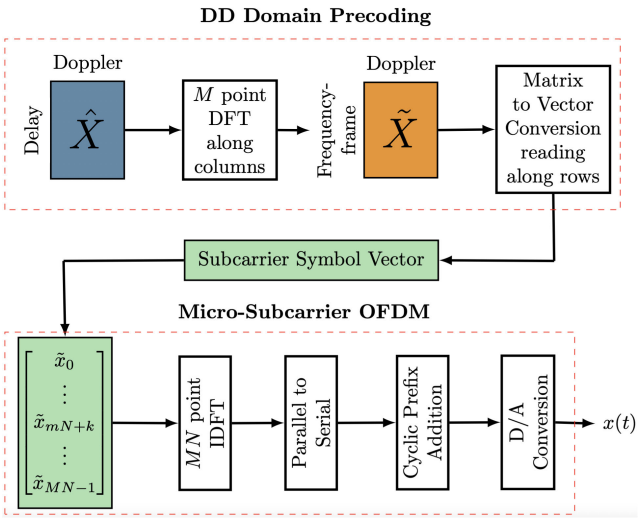

FIGURE 1. Block diagram of DD-OFDM modulation.

indices and $l = 0, \ldots, M-1$ are the delay indices.[2] First, the frequency-Doppler symbols $\tilde{x}_k^{(m)}$ are obtained by taking a DFT along the delay axis of the delay-Doppler data grid according to

$$\tilde{x}_k^{(m)} := \frac{1}{\sqrt{M}} \sum_{l=0}^{M-1} \hat{x}_k^{(l)} e^{-j2\pi \frac{ml}{M}} \tag{4}$$

for $m = 0, \ldots, M-1$ and $l = 0, \ldots, N-1$, where $m = 0, \ldots, M-1$ are the frequency-frame indices. In this representation, the subcarriers $k = 0, \ldots, N-1$ in a frequency-frame m can be interpreted as the Doppler axis (or dimension), and the frequency-frames $m = 0, \ldots, M-1$ as the frequency-frame axis.

As shown in Fig. 2, we place these frequency-frame-Doppler domain symbols on the MN micro-subcarriers, by reading along the frequency-frames, sequentially. Hence, the symbol $\tilde{x}_k^{(m)}$ (obtained in (4)) is placed on subcarrier index $s_k^{(m)}$ defined as

$$s_k^{(m)} := mN + k \tag{5}$$

Note that the micro-subcarriers $\{s_k^{(m)}\}_{k=0}^{N-1}$ form the m^{th} frequency-frame as shown in Fig. 2.

C. DD-OFDM SYMBOL

The transmitted DD-OFDM symbol (3) can be written in terms of the subcarrier indices in (5), as

$$x(t) = \frac{1}{\sqrt{MNT}} \sum_{m=0}^{M-1} \sum_{k=0}^{N-1} \tilde{x}_k^{(m)} e^{j2\pi s_k^{(m)} \frac{\Delta f}{N} t} \tag{6}$$

for $t \in [-T_{cp}, NT)$.

We will analyze the DD-OFDM waveform from the perspective of data carrying DD basis functions. To present the basis functions, we first define the function

$$\mathcal{F}_A(f) := \frac{1}{A} \sum_{a=0}^{A-1} e^{-j2\pi \frac{a}{A} f} \tag{7}$$

for $f \in \mathbb{R}$ and $A \in \mathbb{N}$.

The DD-OFDM symbol in (6) can be expressed using basis functions as follows:

$$x(t) := \sum_{l=0}^{M-1} \sum_{k=0}^{N-1} \hat{x}_k^{(l)} \zeta_k^{(l)}(t), \tag{8}$$

where the basis function $\zeta_k^{(l)}(t)$ that modulates the delay-Doppler data symbol $\hat{x}_k^{(l)}$ is

$$\zeta_k^{(l)}(t) := \frac{1}{\sqrt{NT}} e^{j2\pi k \frac{\Delta f}{N} t} \mathcal{F}_M \left(l - \frac{t}{T/M} \right) \tag{9}$$

for $t \in [-T_{cp}, NT)$, $k = 0, \ldots, N-1$ and $l = 0, \ldots, M-1$.

Theorem 1: The basis functions $\zeta_k^{(l)}(t)$ form an orthonormal set, which satisfies

$$\int_0^{NT} \zeta_k^{(l)}(t) \zeta_{k'}^{*(l')}(t) dt = \frac{1}{M} \delta[k-k'] \delta[l-l'] \tag{10}$$

for $l, l' \in \{0, \ldots, M-1\}$ and $k, k' \in \{0, \ldots, N-1\}$, where $\delta[\cdot]$ is the discrete delta function.

Proof: See Appendix A. □ In the following section, we present a comparison of DD-OFDM with OTFS in terms of the basis functions. We also compare the peak-to-average power ratio (PAPR) and the implemenation complexitites. We will show that the DD-OFDM scheme has identical PAPR, with a slightly higher computational complexity. Later, in Section V, we show that DD-OFDM has lower OOB emission peaks compared to OTFS, and in Sections VIII and IX, we show that DD-OFDM has better channel estimation performance. In Section X, we show that DD-OFDM has better symbol-error rate (SER) and spectral efficiency performance, using numerical simulation.

IV. COMPARISON OF OTFS AND DD-OFDM

In this section, we compare OTFS and DD-OFDM in terms of their basis functions and implementation complexity, highlighting their differences.

The block diagram of OTFS modulation [2] is shown in Fig. 3. By comparing with DD-OFDM in Fig. 1, it can be noted that our DD-OFDM modulation uses a single MN length subcarrier symbol vector and generates a long OFDM symbol of duration NT, whereas OTFS generates N successive OFDM symbols each of which has duration T.

A. BASIS FUNCTIONS

The basis functions $\phi_k^{(l)}(t)$ of OTFS with rectangular pulses are given by

$$\phi_k^{(l)}(t) := \frac{1}{\sqrt{NT}} e^{j2\pi \frac{nk}{N}} \mathcal{F}_M \left(l - \frac{t}{T/M} \right) \tag{11}$$

for $t \in [nT, (n+1)T)$, $n = 0, \ldots, N-1$, $k = 0, \ldots, N-1$ and $l = 0, \ldots, M-1$.

[2]This 2D precoding approach is fundamentally different to standard DFT-precoded OFDM which precodes the data in a single dimension.

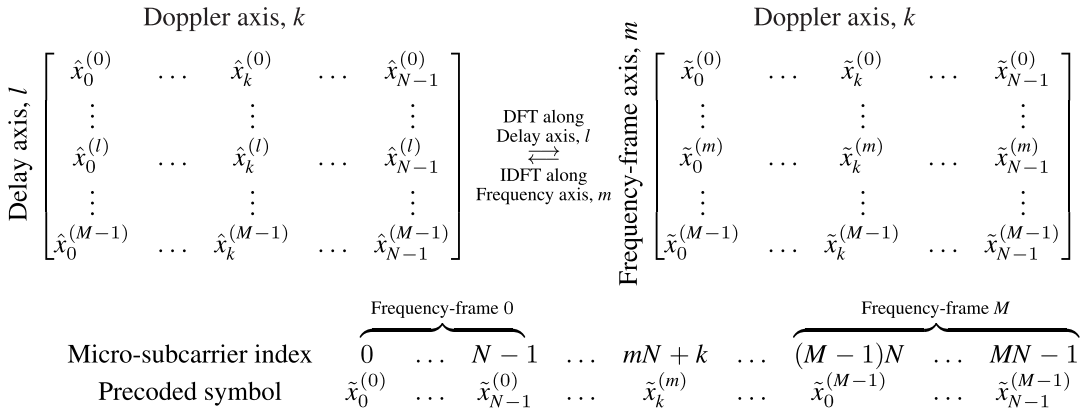

FIGURE 2. Delay-Doppler precoding: Conversion from Delay-Doppler data symbols to micro-subcarrier symbols.

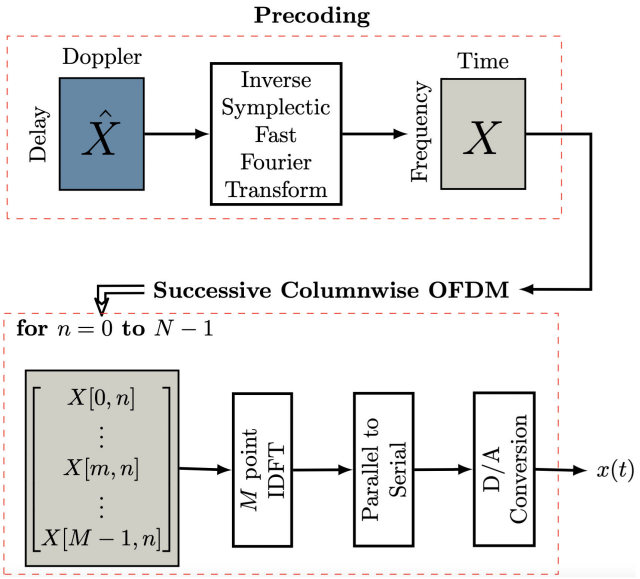

FIGURE 3. Block diagram of OTFS modulation.

By inspection of (9) and (11), we observe that both OTFS and DD-OFDM basis functions have a structure where each basis function is a product of a tone component (see Fig. 4(a)) and a pulse train (see Fig. 4(b)). The tone component for DD-OFDM is the continuous sinusoid $e^{j2\pi\frac{k\Delta f}{N}t}$ whereas OTFS has a piece-wise constant function as a tone which is equal to $\sum_{n=0}^{N-1} e^{j2\pi\frac{kn}{N}}\mathbb{I}_{[nT,(n+1)T)}(t)$, where $\mathbb{I}_S(t)$ is the indicator function which equals 1 if $t \in S$ and 0 otherwise. We note that the tone component of OTFS is a zero order hold approximation of the DD-OFDM tone. We illustrate this in Fig. 4(a).[3]

Both DD-OFDM and OTFS have the same pulse train component, $\mathcal{F}_M(l - \frac{t}{T/M})$, as can be seen from (9) and (11). This is further illustrated in Fig. 4(b) for $t \in [0, NT)$ and $N = 10$.

[3]In Fig. 4 and Fig. 5, we have normalized the gains to be 1 by taking $\frac{1}{\sqrt{NT}} = 1$.

It can be seen from Fig. 4(c) that the difference in the tone component leads to a notable difference in the basis functions for OTFS and DD-OFDM. From Fig. 5, we can also see that the difference between the basis functions does not vanish with larger N. In this paper, we will show that DD-OFDM has lower out-of-band emissions, simpler channel estimation and superior Symbol Error Rate (SER) performance, due to these different basis functions.

B. TIME-DELAY DOMAIN CONVERSION AND IMPLEMENTATION COMPLEXITY

The way that DD-OFDM converts DD domain symbols to Time-Delay (TD) domain symbols (*i.e.* transmitted samples) is also different from the way OTFS does this. In OTFS, the conversion is accomplished by taking an N point DFT along the Doppler axis. In contrast, for DD-OFDM, the relation between the DD and TD symbols is given as

$$x_n^{(l)} = \frac{1}{\sqrt{N}} \sum_{k=0}^{N-1} \hat{x}_k^{(l)} e^{-j2\pi\frac{k}{N}\left(n+\frac{l}{M}\right)} \tag{12}$$

for $n = 0, \ldots, N-1$ and $l = 0, \ldots, M-1$, where we obtain (12) from (8), (9) using the fact that $x_n^{(l)} := \sqrt{T}x(nT + l\frac{T}{M})$ is the l th delay symbol of the n th time frame. It can be noted that conversion to the TD domain in DD-OFDM can be obtained directly by taking a DFT along Doppler axis k on the phase shifted DD symbols $\hat{x}_k^{(l)} e^{-j2\pi\frac{kl}{MN}}$.

We note that TD symbols $\sqrt{T}x(nT + l\frac{T}{M})$ are also the time samples after Parallel to Serial conversion in the DD-OFDM block diagram in Fig. 1. This means that $MN(\log(N) + 1)$ operations are required to obtain the time domain samples of DD-OFDM. Hence, the implementation complexity of DD-OFDM is marginally more than OTFS which requires $MN\log(N)$ operations. However, we will show that the precoding complexity of DD-OFDM allows for much better channel estimation, and superior SER performance.

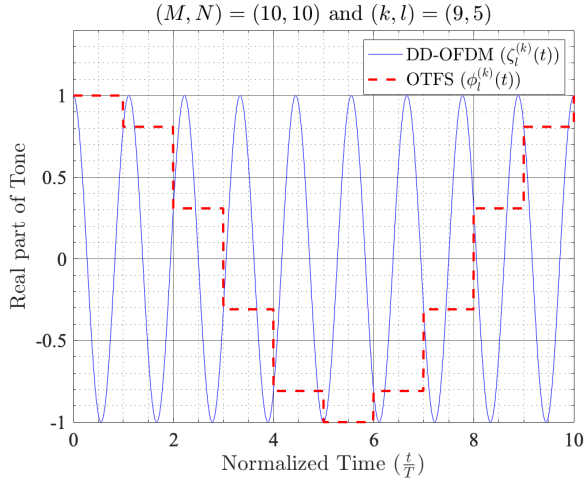

(a) Tone component.

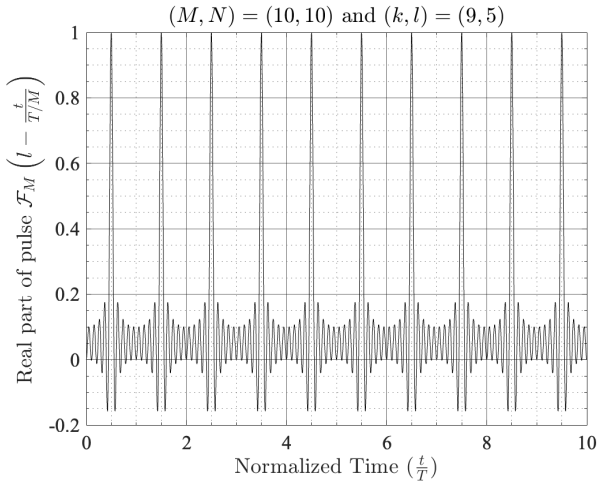

(b) Pulse train component.

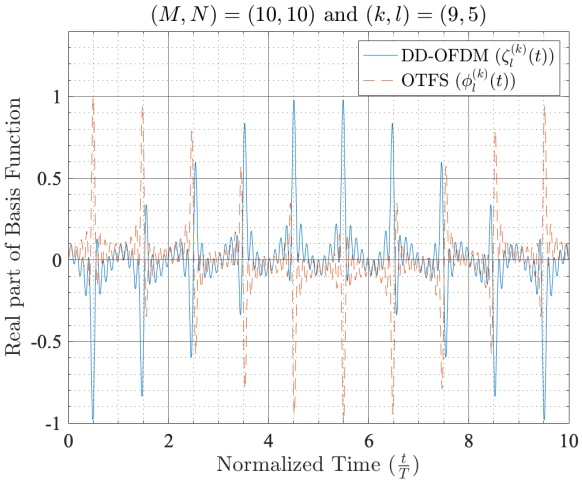

(c) Basis Functions.

FIGURE 4. Comparison of OTFS and DD-OFDM basis functions.

C. PEAK TO AVERAGE POWER RATIO

The PAPR for DD-OFDM is the same as that of OTFS, since the time domain symbols are obtained by a N point DFT of the phase shifted data symbols as shown in (12).

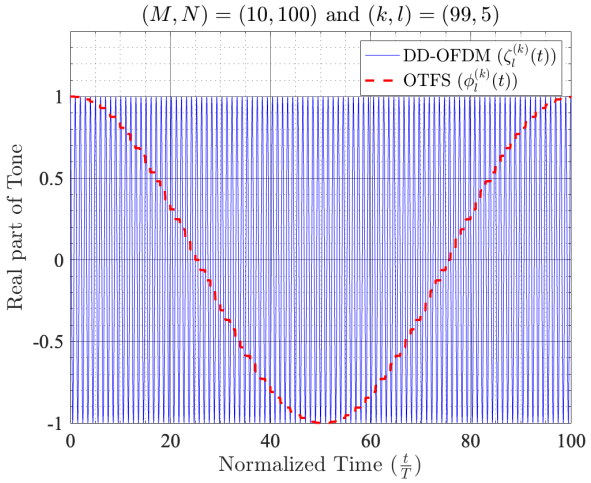

(a) Tone component for $N = 100, k = 99$.

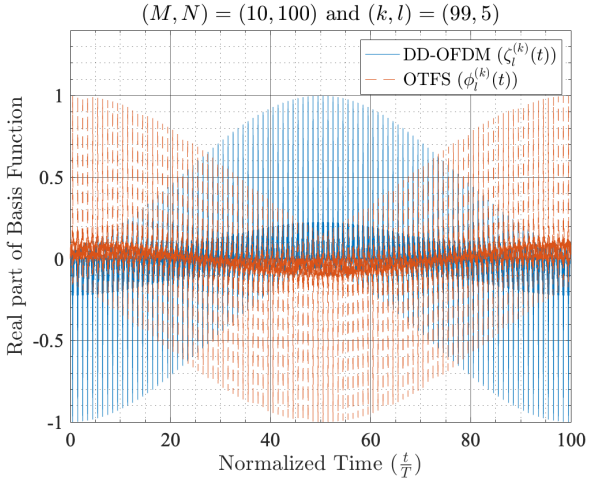

(b) Basis functions for $N = 100, k = 99$.

FIGURE 5. Comparison of OTFS and DD-OFDM basis functions for a larger value of N.

V. OUT OF BAND EMISSIONS

In this section, we show that DD-OFDM has lower out of band (OOB) emissions compared to OTFS.

A. SPECTRA OF BASIS FUNCTIONS

We start with a comparison of the basis functions in the frequency domain. We take a Fourier transform of the basis functions of DD-OFDM and OTFS. Let $Z_k^{(l)}(f) := \frac{1}{\sqrt{NT}} \int_0^{NT} \zeta_k^{(l)}(t) e^{-j2\pi ft} dt$ denote the Fourier transform of the DD-OFDM basis function $\zeta_k^{(l)}(t)$ and $\Phi_k^{(l)}(f) := \frac{1}{\sqrt{NT}} \int_0^{NT} \phi_k^{(l)}(t) e^{-j2\pi ft} dt$ denote the Fourier transform of OTFS basis function $\phi_k^{(l)}(t)$. The magnitude spectra are

$$|Z_k^{(l)}(f)| = \frac{1}{M} \left| \sum_{m=0}^{M-1} e^{-j2\pi \frac{m\left(l - \frac{MN}{2}\right)}{M}} \operatorname{sinc}\left(\frac{f}{\Delta f/N} - (mN + k)\right) \right| \quad (13)$$

$$|\Phi_k^{(l)}(f)| = \left|\mathcal{F}_N\left(\frac{f}{\Delta f/N} - k\right)\right| \frac{1}{M}\left|\sum_{m=0}^{M-1} e^{-j2\pi\frac{m(l-\frac{M}{2})}{M}} \text{sinc}\left(\frac{f}{\Delta f} - m\right)\right| \quad (14)$$

where $|\cdot|$ represents the absolute value.

For DD-OFDM, we note from (13) that the spectrum of the basis functions has the sinc function peaks at $f = m\Delta f + k\frac{\Delta f}{N}$ for $m = 0$ to $M-1$. The magnitudes at these frequencies are $\frac{1}{M}$. Outside the frequency range $[0, M\Delta f]$, there are no spectral peaks for the basis functions and the side-lobes decay quickly as $\text{sinc}(N\frac{f}{\Delta f})$ for every basis function. See Fig. 6(a) for an illustration.

For OTFS, we note from (14) that the basis functions have spectral peaks approximately at the same frequencies as for DD-OFDM. However, the peaks are not constant across the band $[0, M\Delta f]$, as can be seen in Fig. 6(b). Further, the side-lobes of the OTFS basis functions do not decay uniformly outside $[0, M\Delta f]$. For example, for $k = N/2$ (as in Fig. 6(b)) the OTFS basis functions have significant side-lobes at $m\Delta f + \frac{\Delta f}{2}$ for each $m \geq M$ (and $m \leq -1$), where the absolute gain is approximately $\text{sinc}((m - M + 1) + 0.5)$. It is clear that these significant side-lobes decay only as $\text{sinc}(f/\Delta f)$, much slower compared to DD-OFDM. In Fig. 6(b) the most significant side-lobe of OTFS can be observed at $-0.5\Delta f$.

We will now show that this OTFS basis function behaviour, leads to higher expected OOB emission peaks for the OTFS waveform compared to DD-OFDM waveform.

B. EXPECTED OOB EMISSIONS

We define $X(f) := \frac{1}{\sqrt{NT}}\int_0^{NT} x(t)e^{-j2\pi ft}dt$ to be Fourier transform of the DD-OFDM transmitted signal $x(t)$. Recall that $x(t) = \sum_{k=0}^{N-1}\sum_{l=0}^{M-1}\hat{x}_k^{(l)}\zeta_k^{(l)}(t)$.

Similarly, let $X_{\text{otfs}}(f) := \frac{1}{\sqrt{NT}}\int_0^{NT} x_{\text{otfs}}(t)e^{-j2\pi ft}dt$ be the Fourier transform of the OTFS transmitted signal $x_{\text{otfs}}(t) = \sum_{k=0}^{N-1}\sum_{l=0}^{M-1}\hat{x}_k^{(l)}\phi_k^{(l)}(t)$.

Our following theorem presents the expected power spectral density of the two waveforms.

Theorem 2: Suppose that the data symbols $\hat{x}_k^{(l)}$'s are independent and identically distributed (i.i.d) random variables, satisfying $\mathbb{E}[|\hat{x}_k^{(l)}|^2] = 1$ and $\mathbb{E}[\hat{x}_k^{(l)}] = 0$. The expected value of the power spectral density of DD-OFDM signal is given by

$$\mathbb{E}[|X(f)|^2] = \frac{1}{M}\sum_{m=0}^{M-1}\sum_{k=0}^{N-1} sinc^2\left(\frac{f}{\Delta f/N} - (mN+k)\right) \quad (15)$$

whereas for the OTFS signal, it is given by

$$\mathbb{E}[|X_{otfs}(f)|^2] = \frac{1}{M}\sum_{m=0}^{M-1} sinc^2\left(\frac{f}{\Delta f} - m\right) \quad (16)$$

Proof: See Appendix A. □

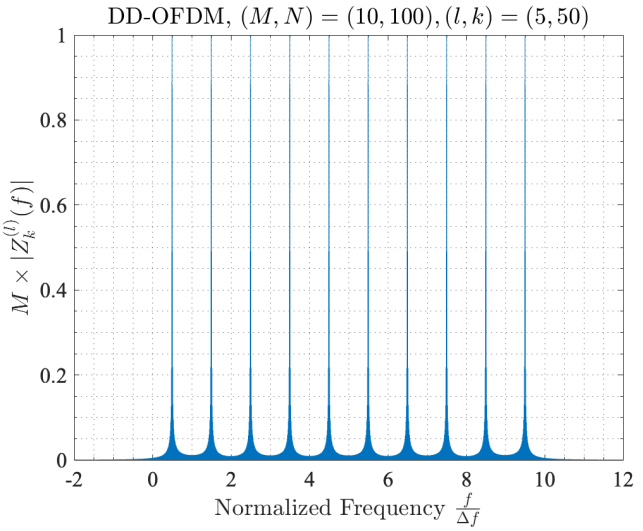

(a) DD-OFDM basis function's power spectrum.

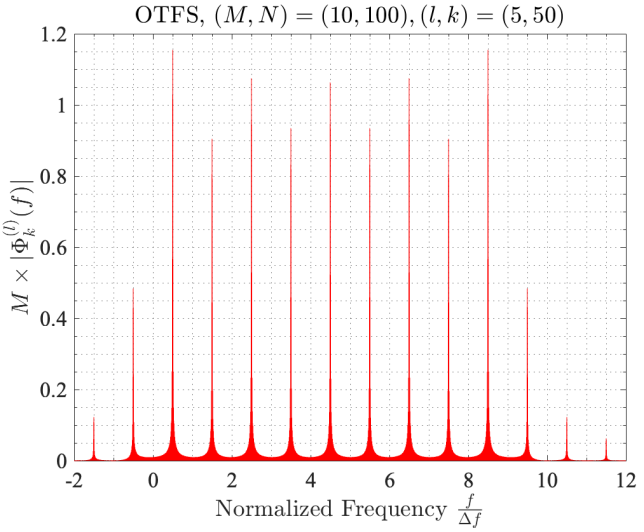

(b) OTFS basis function's power spectrum.

FIGURE 6. Power spectrum comparison for DD-OFDM and OTFS basis functions.

From Theorem 2, it can be noted the expected power spectral density of OTFS is equivalent to an OFDM waveform with M subcarriers with subcarrier spacing Δf. It can also be noted that the expected power spectral density of DD-OFDM is equivalent to an OFDM waveform with MN subcarriers with subcarrier spacing $\frac{\Delta f}{N}$. Hence, the side lobes of DD-OFDM signal decay approximately as $N\text{sinc}^2(N\frac{f}{\Delta f})$, whereas the OTFS signal side lobes decay as $\text{sinc}^2(\frac{f}{\Delta f})$. Hence, the OOB emission peaks for DD-OFDM is of the order N times lower than that of OTFS.

Fig. 7 shows the power spectral density of both DD-OFDM, and OTFS, for $N = 50$ and $M = 250$. As predicted, OOB emission peaks of DD-OFDM are approximately 18 dB smaller than OTFS.

VI. FREQUENCY DOMAIN CYCLIC REPLICATION

In this section, we propose a cyclic replication of a small number of the micro subcarrier symbols for DD-OFDM,

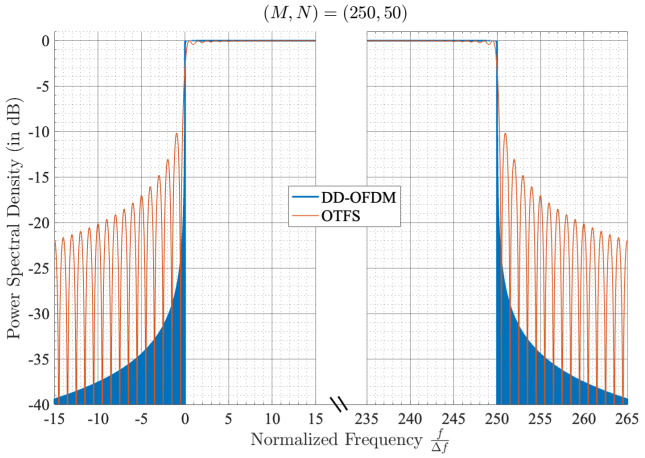

FIGURE 7. Comparison of OOB emission peaks.

which allows for a simpler baseband model that will be presented in the next section.

Notice that the transmitted signal undergoes doubly dispersive fading, as in (2), before reaching the receiver and that the Doppler shifts are in the range $[-\frac{\nu_{\max}}{2}, \frac{\nu_{\max}}{2}]$. To compensate for energy loss out of band due to Doppler, and to simplify the receiver processing, we add cyclic subcarriers in the frequency domain around the DD-OFDM symbol.[4]

We add N_g additional micro-subcarriers on either side of the MN DD-OFDM micro-subcarriers, and fill them in a cyclic manner. On the lower frequency side, we add a subframe of N_g micro-subcarriers, and similarly on the upper frequency side, resulting in $MN + 2N_g$ micro-subcarriers:

$$s_{N-N_g}^{(-1)} \dots s_{N-1}^{(-1)} \; s_0^{(0)} \dots s_{N-1}^{(0)} \; \dots \; \dots \; s_0^{(M-1)} \dots s_{N-1}^{(M-1)} \; s_0^{(M)} \dots s_{N_g-1}^{(M)} \tag{17}$$

For the subcarrier symbols on the lower subframe (indexed by $m = -1$), we copy the subcarrier symbols from frequency-frame $M-1$, *i.e.* $\tilde{x}_{N-k}^{(-1)} := \tilde{x}_{N-k}^{(M-1)}$, for $k = 1, 2, \dots, N_g$. Similarly, for the subcarrier symbols on the upper subframe (indexed by $m = M$), we copy the subcarrier symbols from frequency-frame 0, i.e. $\tilde{x}_k^{(M)} := \tilde{x}_k^{(0)}$, for $k = 0, 1, \dots, N_g - 1$.

This gives the following ordering of micro-subcarrier symbols across the $MN + 2N_g$ micro-subcarriers:

$$\tilde{x}_{N-N_g}^{(M-1)} \dots \tilde{x}_{N-1}^{(M-1)} \; \tilde{x}_0^{(0)} \dots \tilde{x}_{N-1}^{(0)} \; \dots \; \dots \; \tilde{x}_0^{(M-1)} \dots \tilde{x}_{N-1}^{(M-1)} \; \tilde{x}_0^{(0)} \dots \tilde{x}_{N_g-1}^{(0)} \tag{18}$$

which clearly shows the cyclic replication. The value N_g is chosen such that $2N_g \frac{\Delta f}{N}$ is greater than the Doppler spread of the channel $\nu_{\max}$. The block diagram for DD-OFDM including the cyclic replication of micro-subcarrier symbols

[4]The idea of a frequency domain cyclic prefix was first proposed for OFDM in [25] but it was for time dispersive channels. In contrast, our waveform is for DD domain communication in doubly dispersive channels. We also note that cyclic subcarriers are not strictly necessary for DD-OFDM (see Appendix B).

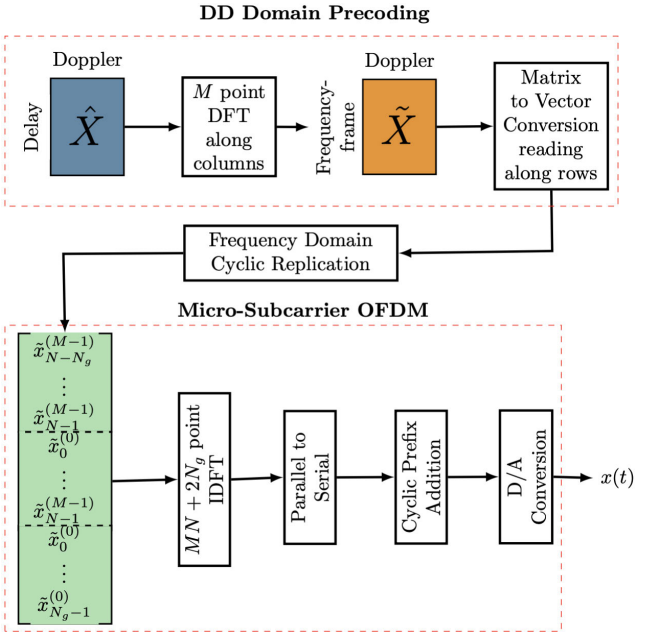

FIGURE 8. DD-OFDM block diagram with frequency domain cyclic replication of N_g micro subcarrier symbols on either side.

is shown in Fig. 8. As explained, the symbols in (18) form the subcarrier symbol vector (shown in green color) of the Micro-Subcarrier OFDM block.

Remark 1: Cyclic replication on both sides is used since Doppler shifts can take either positive or negative values. In contrast, cyclic repetition is used in the time domain to deal with delay spread (as in standard OFDM) and then a cyclic prefix suffices due to delays being non-negative.

A. IMPACT ON SPECTRAL EFFICIENCY

The spectral efficiency (transmitted symbols/sec/Hz) depends on the following factors: the DD grid size (M, N), the frequency cyclic replication length N_g, and the time domain cyclic prefix length N_d. The time-bandwidth product is given by

$$\left(NT + N_d \frac{T}{M}\right)\left(M\Delta f + 2N_g \frac{\Delta f}{N}\right) = MN + 2N_g + N_d + \frac{2N_g N_d}{MN} \tag{19}$$

The term $\frac{2N_g N_d}{MN}$ can be ignored, since it is smaller than 1 and hence much smaller than $MN + 2N_g + N_d$. Therefore, the spectral efficiency is

$$\frac{MN}{MN + 2N_g + N_d} \tag{20}$$

This expresssion includes the frequency domain cyclic replication and time domain cyclic prefix.

Note that (20) can be expressed as

$$\left(1 + \frac{1}{M}\frac{2N_g}{N} + \frac{1}{N}\frac{N_d}{M}\right)^{-1} \approx \left(1 + \frac{\nu_{\max}}{M\Delta f} + \frac{\tau_{\max}}{NT}\right)^{-1}$$

Clearly the spectral efficiency is close to 1, when the Doppler spread $\nu_{\max}$ is small in comparison to DD-OFDM's bandwidth $M\Delta f$, and the delay spread $\tau_{\max}$ is small in comparison to the symbol time NT.[5]

VII. DELAY-DOPPLER DOMAIN RECEIVER

In this section, we present the receiver for our DD-OFDM waveform and derive the baseband I/O relation for DD-OFDM in an integer Doppler channel. We then consider the general case of non-integer fractional Doppler channels, using the same receiver.

A. RECEIVER

For sake of convenience, let $l_p := \frac{\tau_p}{T/M}$ and $k_p := \frac{\nu_p}{\Delta f/N}$ denote the normalized delay and Doppler shift for each path $p = 0, \ldots, P-1$. We take l_p to be an integer in the current section. Later in Section IX, we will generalize to the case of non-integer delays.

We employ a matched filtering receiver utilizing the orthogonality of the DD-OFDM basis functions. The DD received symbol $\hat{y}_{k'}^{(l')}$ is the matched filtering output of the received waveform $y(t)$ with the basis function $\zeta_{k'}^{*(l')}(t)$ as given by

$$\hat{y}_{k'}^{(l')} := \int_0^{NT} y(t)\zeta_{k'}^{*(l')}(t)dt \tag{21}$$

$$= \frac{1}{\sqrt{M}} \sum_{m=0}^{M-1} e^{j2\pi \frac{ml'}{M}} \tilde{y}_{mN+k'} \tag{22}$$

for $k' = 0, \ldots, N-1$ and $l' = 0, \ldots, M-1$, where

$$\tilde{y}_{mN+k'} := \frac{1}{\sqrt{MNT}} \int_0^{NT} y(t) e^{-j2\pi (mN+k')\frac{\Delta f}{N} t} dt \tag{23}$$

is received symbol for subcarrier $mN + k'$.

From (22), we note that matched filtering with DD-OFDM basis functions is equivalent to taking an IDFT along the frequency-frame dimension m on the received OFDM subcarrier symbols. Hence, we first focus on obtaining the subcarrier symbols. The transmitted signal is $x(t) = \sum_{s=-N_g}^{MN+N_g-1} \tilde{x}_s e^{j2\pi s \frac{\Delta f}{N} t}$ with the cyclic symbols in (18). Substituting $x(t)$ in (2), the received signal $y(t)$ is

$$y(t) = \sum_{p=0}^{P-1} \sum_{s=-N_g}^{MN+N_g-1} h_p e^{-j2\pi \frac{s\Delta f}{N}\tau_p} e^{j2\pi (s+k_p)\frac{\Delta f}{N} t} \tilde{x}_s. \tag{24}$$

Hence, evaluating the Fourier transform in (23) of $y(t)$ from 0 to NT, we obtain the received subcarrier symbols as

$$\tilde{y}_{mN+k'} = \sum_{p=0}^{P-1} \sum_{s=-N_g}^{MN+N_g-1} h'_p e^{-j2\pi \frac{sl_p}{MN}} \tilde{x}_s e^{j\pi (s-mN-k'+k_p)} \operatorname{sinc}\left(s - (mN + k' - k_p)\right) \tag{25}$$

[5]Note that in contrast, the spectral efficiency of standard OFDM is $\approx \left(1 + \frac{\tau_{\max}}{T}\right)^{-1}$, where $\frac{\tau_{\max}}{T} \gg \frac{\tau_{\max}}{NT}$ for large N. Hence, the wider subcarrier OFDM is more susceptible to delay spread compared to DD-OFDM, as mentioned in Section I.

for $m = 0, \ldots, M-1$ and $k' = 0, \ldots, N-1$, where, $h'_p := \frac{h_p}{M}$.

B. INTEGER DOPPLER CHANNEL

We denote $\tilde{y}_{k'}^{(m)} := \tilde{y}_{mN+k'}$ using the frequency-frame-Doppler representation. For an integer Doppler channel, *i.e.* k_p's are integers, note that $\operatorname{sinc}(s - (mN + k' - k_p)) = \delta[s - (mN + k' - k_p)]$ in (25). Hence, the received micro-subcarrier symbols are

$$\tilde{y}_{k'}^{(m)} := \sum_{p=0}^{P-1} h'_p e^{-j2\pi (mN+k'-k_p)\frac{l_p}{MN}} \tilde{x}[m, k' - k_p] \tag{26}$$

where

$$\tilde{x}[m,k] := \begin{cases} \tilde{x}_k^{(m)} & \text{if } k \in [0, N-1] \\ \tilde{x}_{(k)_N}^{(m-1)_M} & \text{if } k < 0 \\ \tilde{x}_{(k)_N}^{(m+1)_M} & \text{if } k > N-1 \end{cases} \tag{27}$$

and where $(m)_M := m \mod M$, and $(k)_N := k \mod N$. The modulo operation arises because of the cyclic structure of the data sequence, as in (18).

Using (26) and (4), from (22), we obtain the DD domain baseband I/O equation for the integer Doppler channel as

$$\hat{y}_{k'}^{(l')} = \sum_{p=0}^{P-1} \hat{h}'_p e^{-j2\pi \frac{k'l_p}{MN}} \sum_{l=0}^{M-1} \mathcal{F}_M(l_p - l' + l)\hat{x}[l, k' - k_p] \tag{28}$$

where $\hat{h}'_p = h'_p e^{j2\pi \frac{k_p l_p}{MN}}$ and

$$\hat{x}[l,k] := \begin{cases} \hat{x}_k^{(l)} & \text{if } k \in [0, N-1] \\ e^{j2\pi \frac{l}{M}} \hat{x}_{(k)_N}^{(l)} & \text{if } k < 0 \\ e^{-j2\pi \frac{l}{M}} \hat{x}_{(k)_N}^{(l)} & \text{if } k > N-1 \end{cases} \tag{29}$$

Recall that $\hat{x}_k^{(l)}$ are the data symbols which were placed on the delay-Doppler grid, and in (29) we see that some of them are phase rotated.

Since l_p's are integers, $\mathcal{F}_M\left(l_p - l' + l\right) = \delta[(l_p - l' + l)_M]$, by the definition in (7). Hence, (28) can be written as

$$\hat{y}_{k'}^{(l')} = \sum_{p=0}^{P-1} \hat{h}'_p e^{-j2\pi \frac{k'l_p}{MN}} \hat{x}[(l' - l_p)_M, k' - k_p] \tag{30}$$

Note that the above twisted convolution equation has a path delay dependent phase compensation term $e^{-j2\pi \frac{k'l_p}{MN}}$ in contrast to OTFS where path Doppler shift dependent phase compensation appears in the twisted convolution [6], [11], as

$$\hat{y}_{k'}^{(l')} = \sum_{p=0}^{P-1} \hat{h}'_p e^{j2\pi \frac{l'k_p}{MN}} \hat{x}_{(k'-k_p)_N}^{(l'-l_p)_M} \tag{31}$$

for $l' \geq \max_p l_p$. Recall that $\hat{x}_{(k'-k_p)_N}^{(l'-l_p)_M}$ are the delay-Doppler data symbols and note that the OTFS phase compensation term $e^{j2\pi \frac{l'k_p}{MN}}$ depends on path Doppler shifts. In an integer Doppler channel, the path Doppler shifts can be obtained

from the Doppler taps *i.e.* measurements on the integer grid points. However, non-integer Doppler channels must be considered due to the low Doppler resolution in practical implementations. In non-integer Doppler channels, the path Doppler shifts cannot be measured directly from the taps and hence channel estimation for OTFS is a challenging problem in non-integer Doppler channels.

In the next section, we will consider a general non-integer Doppler channel and show that a similar baseband I/O relationship holds for DD-OFDM, where the phase compensation term depends only on the path delays. We will also present a practical channel estimation scheme which utilizes this structure of our DD-OFDM baseband model.

C. NON-INTEGER DOPPLER CHANNEL

For the non-integer Doppler case, there is more Doppler spread in the baseband due to side-lobes of the sinc function. We choose a sufficiently large number of cyclic micro-subcarriers to deal with the spread of the sinc function, as follows. Let $\lfloor x \rfloor$ denote the largest integer that is smaller than or equal to x. We suppose that $N_g \geq \max_p \lfloor k_p \rfloor + S$, where $S \in \mathbb{N}$ is the value for which $\text{sinc}(x) \approx 0$ for $|x| > S$, *e.g.* $|\text{sinc}(x)| \leq 0.016$ for $|x| \geq 20$. Hence, we will ignore the values of sinc function outside the range $[-S, S]$ in (25). This approximation leads to an ISI term which has magnitude of the order $\frac{1}{\pi S}$, which can be ignored. Note that $S < N_g < N$, since N is large. Similar approximations were used in [4] and [5] for non-integer fractional Doppler models of OTFS.

We present our main result on DD-OFDM baseband equations for practical non-integer Doppler channels in the following Theorem 3.

Theorem 3: The DD-OFDM baseband equations for a general non-integer Doppler channel are

$$\hat{y}_{k'}^{(l')} = \sum_{p=0}^{P-1} \sum_{i=-N_g}^{N_g} \hat{h}_p[i] e^{-j2\pi \frac{k' l_p}{MN}} \hat{x}[(l'-l_p)_M, k'-i] \quad (32)$$

where $\hat{h}_p[i] := h'_p e^{j\pi(k_p - i)} e^{j2\pi \frac{i l_p}{MN}} \text{sinc}(k_p - i)$ *is the gain corresponding to Doppler tap i of path p with delay tap* l_p.

Proof: See Appendix A. □

As can be seen from (32) in Theorem 3, the phase compensation term for DD-OFDM in the non-integer Doppler channel only depends on the path delays. Here, each path p gives rise to multiple Doppler taps $i = -N_g$ to N_g in contrast to the integer Doppler channel, where each path results in a single Doppler tap. In the non-integer channel, the tap gains $\hat{h}_p[i]$'s have to be estimated in order to construct the DD domain baseband channel matrix. However, for the phase compensation term in the channel coefficient, only path delays need to be estimated and not Doppler shifts. As explained in the introduction, path delays are much easier to estimate than path Doppler shifts due to the better resolution that exists in the delay dimension of the DD grid. This is a real, practical advantage of DD-OFDM over OTFS. In the next section, we show how to estimate the tap gains in DD-OFDM.

VIII. CHANNEL ESTIMATION FOR DD-OFDM

In this section, we describe a practical channel estimation scheme for DD-OFDM. We consider the high-SNR regime to highlight the effect of the unknown phase compensation term and the number of considered taps. We apply the same method to OTFS and compare the two schemes.

A. CHANNEL ESTIMATION SCHEME

Consider the pilot scheme in [5], (which considered OTFS with rectangular pulses, but did not consider fractional Doppler channels), where a pilot symbol is placed at location (l_1, k_1) and surrounded by guard bands.

$$\hat{x}_k^{(l)} = \begin{cases} 1 & \text{if } l = l_1 \text{ and } k = k_1 \\ 0 & \text{if } (l,k) \neq (l_1,k_1), |l-l_1| \leq l_{\max}, \\ & \text{and } |k-k_1| \leq 2N_g \end{cases} \quad (33)$$

We suppose (l_1, k_1) is chosen such that $l_{\max} \leq l_1$ and $N_g \leq k_1 \leq N - N_g - 1$ so that $l_1 - l_{\max} \geq 0$ and $k_1 \pm N_g \in \{0, \ldots, N-1\}$. Ignoring noise, we obtain from (32) that

$$\hat{y}_k^{(l)} = \sum_{p=0}^{P-1} \sum_{i=-N_g}^{N_g} \hat{h}_p[i] e^{-j2\pi \frac{k l_p}{MN}} \hat{x}_{k-i}^{(l-l_p)} \quad (34)$$

for $l \in \{l_1, \ldots, l_1 - l_{\max}\}$ and $k \in \{k_1 - N_g, \ldots, k_1 + N_g\}$. Note that by pilot design $\hat{x}_{k-i}^{(l-l_p)} = 1$ only if $l - l_p = l_1$ and $k + i = k_1$, *i.e.* $\hat{x}_{k-i}^{(l-l_p)} = \delta[l - (l_1 + l_p)]\delta[k - (k_1 + i)]$. Hence from (34), we obtain the impulse response equation for DD-OFDM as

$$\begin{aligned} \hat{y}_k^{(l)} &= \sum_{p=0}^{P-1} \sum_{i=-N_g}^{N_g} \hat{h}_p[i] e^{-j2\pi \frac{k l_p}{MN}} \delta[l - (l_1 + l_p)]\delta[k - (k_1 + i)] \\ &= \sum_{p=0}^{P-1} \sum_{i=-N_g}^{N_g} \hat{h}_p[i] e^{-j2\pi \frac{k(l-l_1)}{MN}} \delta[l - (l_1 + l_p)]\delta[k - (k_1 + i)] \end{aligned} \quad (35)$$

where (35) follows since l_p is an integer.

The observed symbol $\hat{y}_{k_1+i}^{(l_1+l_p)}$ at the grid location $(l_1 + l_p, k_1 + i)$ has the value $\hat{h}_p[i] e^{-j2\pi \frac{(k_1+i) l_p}{MN}}$. Hence using (35), $\hat{h}_p[i]$'s and l_p's can be obtained directly from the DD baseband channel impulse response.

The DD domain channel coefficient for each transmitted and received symbol pair $(x_k^{(l)}, y_{k'}^{(l')})$ can be computed using $\hat{h}_p[i]$'s and l_p's as seen from the DD base-band equation (32) in Theorem 3. Hence, the presented practical channel estimation scheme can be used to perfectly construct the full DD baseband channel matrix.

This approach for DD-OFDM channel estimation is practical since it directly utilizes the baseband impulse response, and does not require additional knowledge such as the number of individual paths, or additional processing

to obtain path level information. We can simply treat each delay-Doppler tap at delay index l_p and the Doppler index i, as an individual effective path with Doppler $i\frac{\Delta f}{N}$, delay $l_p\frac{T}{M}$ and gain $\hat{h}_p[i]$. No error is incurred by this approach as can be seen from the DD-OFDM base-band relation in (32). The accuracy of the constructed channel matrix depends only on the number of considered Doppler taps, $2N_g+1$, where $N_g = S + \max_p \lfloor k_p \rfloor$ is the number of guard symbols.

Note that this efficient channel estimation approach for non-integer fractional Doppler channels can also be taken for OTFS, however, it cannot achieve the same overall accuracy as DD-OFDM (as will be shown in Section VIII-B). For OTFS, a significant error is incurred during the channel matrix construction, since the phase compensation term for OTFS is computed using the integer Doppler tap values instead of the path Doppler shift.

The baseband equations for OTFS are given by [6] as

$$\begin{aligned}\hat{y}_{k'}^{(l')} &= \sum_{p=0}^{P-1} h'_p e^{j2\pi\frac{l'}{M}\frac{k_p}{N}} \sum_{l=0}^{M-1}\sum_{k=0}^{N-1} \mathcal{F}_M(l_p - l' + l) \\ &\quad \mathcal{F}_N(k'-k-k_p)\hat{x}_k^{(l)} e^{-j2\pi\frac{k'-k_p}{N}\mathbf{1}(l'<l_p)} \qquad (36)\\ &= \sum_{p=0}^{P-1} h'_p e^{j2\pi\frac{l'}{M}\frac{k_p}{N}} \sum_{k=0}^{N-1} \mathcal{F}_N(k'-k-k_p)\hat{x}_k^{(l'-l_p)_M} \\ &\quad e^{-j2\pi\frac{k'-k_p}{N}\mathbf{1}(l'<l_p)} \qquad (37)\end{aligned}$$

where $\mathbf{1}(\cdot)$ is the indicator function.

For comparison, we consider OTFS with full cyclic prefix (OTFS-FCP) [11], where cyclic prefix symbols are used in the delay-Doppler frame, which is equivalent to adding a time-domain cyclic prefix at the beginning of each OTFS frame. This is in contrast to OTFS with reduced cylic prefix (OTFS-RCP), where only a single time-domain cyclic prefix is added at beginning of the entire OTFS symbol. For FCP, the data symbols $\hat{d}_k^{(l)}$ for $l = 0,\ldots,M-M_{cp}-1$ and $k = 0,\ldots,N-1$, are placed on delay indices $l+M_{cp}$ for each Doppler index k (*i.e.* $\hat{x}_k^{(l)} = \hat{d}_k^{(l-M_{cp})}$ for $l = M_{cp},\ldots,M-1$). The rest of the delay indices $l = 0\ldots M_{cp}-1$ are cyclic prefix symbols, *i.e.* $\hat{x}_k^{(l)} = \hat{d}_k^{(l-M_{cp}+M)}$. We denote the received symbols $\hat{r}_{k'}^{(l')} := \hat{y}_{k'}^{(l'+M_{cp})}$ for $l' = 0,\ldots,M-M_{cp}-1$ and $k' = 0,\ldots,N-1$.

By considering S significant side-lobes of the $\mathcal{F}_N(\cdot)$ function and using the cyclic prefix symbols, we obtain (38) from (37). Further, approximating the path phase compensation term $e^{j2\pi\frac{l'k_p}{MN}}$ in (38) with the phase rotation $e^{j2\pi\frac{l'i}{MN}}$ based on the Doppler tap i, in (39), we obtain the Doppler tap model for OTFS as

$$\hat{r}_{k'}^{(l')} \approx \sum_{p=0}^{P-1} h'_p e^{j2\pi\frac{l'}{M}\frac{k_p}{N}} \sum_{i=\lfloor k_p\rfloor-S}^{\lfloor k_p\rfloor+S} \mathcal{F}_N(i-k_p)\hat{d}_{(k'-i)_N}^{(l'-l_p)_{M-M_{cp}}} \qquad (38)$$

$$\begin{aligned}&\approx \sum_{p=0}^{P-1}\sum_{i=\lfloor k_p\rfloor-S}^{\lfloor k_p\rfloor+S} h'_p e^{j2\pi\frac{l'}{M}\frac{i}{N}} \mathcal{F}_N(i-k_p)\hat{d}_{(k'-i)_N}^{(l'-l_p)_{M-M_{cp}}} \\ &= \sum_{p=0}^{P-1}\sum_{i=-N_g}^{N_g} g_p[i] e^{j2\pi\frac{l'}{M}\frac{i}{N}} \hat{d}_{(k'-i)_N}^{(l'-l_p)_{M-M_{cp}}} \qquad (39)\end{aligned}$$

where $g_p[i] := h'_p \mathcal{F}_N\left(i-k_p\right)$ for $i = \lfloor k_p\rfloor - S,\ldots,\lfloor k_p\rfloor + S$, and recall that $N_g = \max_p\lfloor k_p\rfloor + S$. Note that approximating path phase rotation $e^{j2\pi\frac{l'k_p}{MN}}$ in (38) with the tap phase rotation $e^{j2\pi\frac{l'i}{MN}}$ in (39), results in a phase compensation error for OTFS Doppler tap model.

B. COMPARISON OF CHANNEL ESTIMATION ERROR

In this subsection, we compare the accuracy of our channel estimation scheme for DD-OFDM and OTFS treating each tap in the impulse response as an individual path with the corresponding observed gain.

Consider the vectorized input-output relations as $\boldsymbol{y} = H\boldsymbol{x}$, where $\boldsymbol{y}(l'N+k') = \hat{y}_{k'}^{(l')}$, $\boldsymbol{x}(lN+k) = \hat{x}_k^{(l)}$ and H is the full channel matrix when all the Doppler taps are considered. Let H_{N_g} be the channel coefficient when the Doppler taps from $-N_g$ to N_g are considered. $H_{N_g}(l'N+k', lN+k)$ can be computed from (32), using the knowledge of channel impulse response in (35) as explained in the previous section.

We define the normalized mean square error (NMSE) as

$$\text{NMSE}(N_g) := \frac{\|H - H_{N_g}\|^2}{\|H\|^2} \qquad (40)$$

where $\|\cdot\|$ represents the Frobenius norm of a matrix.

We compare the normalized mean square error (NMSE) incurred by using the integer Doppler path approximation for both OTFS and DD-OFDM.

Following [5] and [13], we consider the 3GPP EVA model for the power delay profile [26], with delays rounded to the nearest integer taps, and a Jakes model for the path Doppler shifts. We consider a receiver speed of 200 kmph and a carrier frequency of 4 GHz, and the parameter values $M = 500, N = 100$ and $\Delta f = 15$ kHz for both DD-OFDM and OTFS waveforms. $M_{cp} = 19$ for OTFS. The presented NMSE values are averaged over 10^3 channel realizations.

It can be seen from Fig. 9 that DD-OFDM channel estimation is much more accurate in non-integer Doppler channels. Hence, the proposed practical channel estimation scheme which directly uses the channel impulse response is sufficient for DD-OFDM, unlike OTFS where more sophisticated methods with additional processing complexity are required to achieve the same reconstruction accuracy.

IX. THE NON-INTEGER DELAY AND NON-INTEGER DOPPLER CHANNEL

In this section we consider the general case of non-integer fractional path delays, and show that our DD-OFDM scheme maintains its advantages over OTFS in this general case.

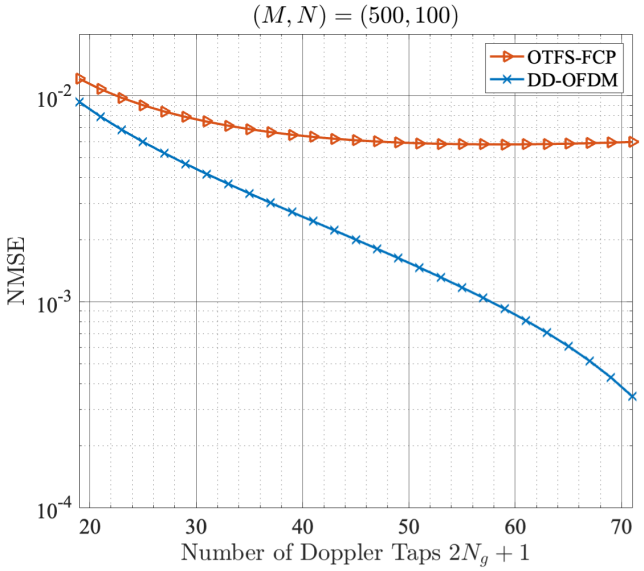

FIGURE 9. Channel estimation error in fractional non-integer Doppler channel.

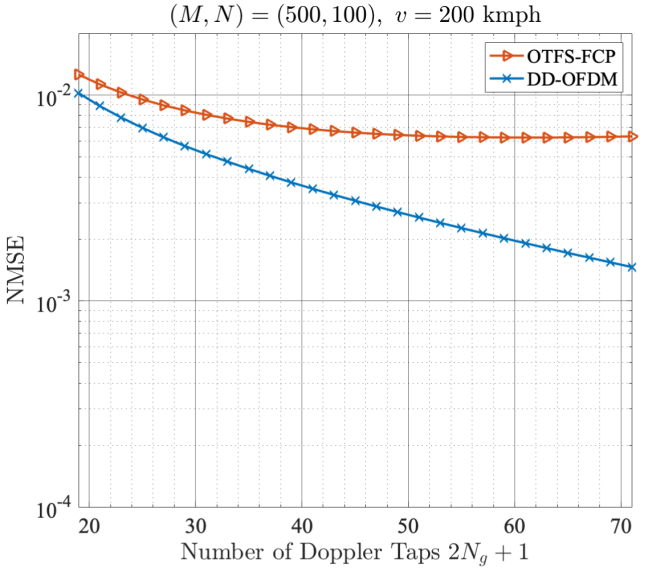

FIGURE 10. Channel estimation error with fractional non-integer delay and non-integer Doppler channel for UE speed $v = 200$ kmph.

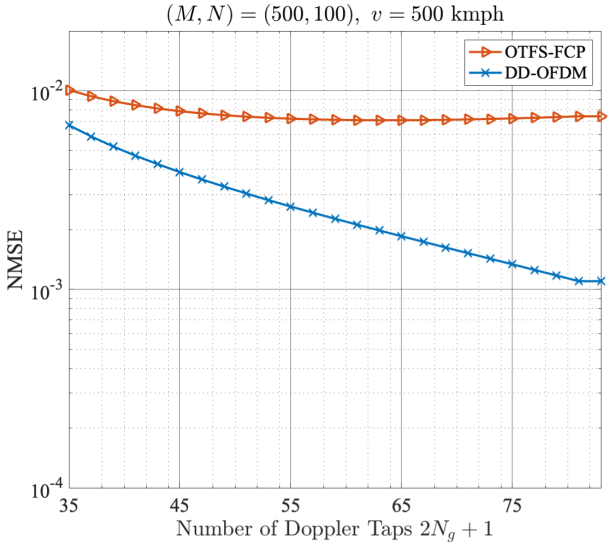

FIGURE 11. Channel estimation error with fractional non-integer delay and non-integer Doppler channel for UE speed $v = 500$ kmph.

In doing so, we provide extra support and insight into how high delay resolution (or equivalently wide signal bandwidth) leads to an integer delay tap model for DD-OFDM.

A. DD-OFDM WITH NON-INTEGER FRACTIONAL PATH DELAYS AND FRACTIONAL DOPPLER SHIFTS

For a non-integer fractional delay channel where l_p's are not integers, we can write the DD-OFDM base band equations as

$$\hat{y}^{(l')}_{k'} = \sum_{p=0}^{P-1} \sum_{i=-N_g}^{N_g} \hat{h}'_p[i] e^{-j2\pi \frac{k'}{N} \frac{l_p}{M}} \sum_{l=0}^{M-1} \mathcal{F}_M(l_p - l' + l) \hat{x}[l, k' - i] \tag{41}$$

By considering (only) the S_d significant side-lobes of the $\mathcal{F}_M(\cdot)$ function, we can write

$$\begin{aligned} \hat{y}^{(l')}_{k'} &\approx \sum_{p=0}^{P-1} \sum_{s=-S_d}^{S_d} \sum_{i=-N_g}^{N_g} \hat{h}'_p[\lfloor l_p \rfloor + s, i] e^{-j2\pi \frac{k'}{N} \frac{l_p}{M}} \\ &\quad \hat{x}[l' - \lfloor l_p \rfloor - s, k' - i] \\ &= \sum_{p=0}^{P-1} \sum_{q=\lfloor l_p \rfloor - S_d}^{\lfloor l_p \rfloor + S_d} \sum_{i=-N_g}^{N_g} \hat{h}'_p[q, i] e^{-j2\pi \frac{k'}{N} \frac{l_p}{M}} \hat{x}[l' - q, k' - i] \end{aligned} \tag{42}$$

where $\hat{h}'_p[q, i] := \hat{h}'_p[i] \mathcal{F}_M(l_p - q)$ for $q = \lfloor l_p \rfloor - S_d, \ldots, \lfloor l_p \rfloor + S_d$, and 0 otherwise.

Note that M is very large due to wide bandwidth, and hence $|q - \lfloor l_p \rfloor| = |s| \leq S_d \ll M$ for each $q \in \{\lfloor l_p \rfloor - S_d, \ldots, \lfloor l_p \rfloor + S_d\}$. Hence, $\frac{q - l_p}{M} = \frac{s}{M} + \frac{\lfloor l_p \rfloor - l_p}{M} \approx 0$, which means that all the paths p which contribute to a delay tap q (*i.e.* $|\lfloor l_p \rfloor - q| \leq S$) have nearly the same phase compensation term, $e^{-j2\pi \frac{k'}{N} \frac{l_p}{M}} \approx e^{-j2\pi \frac{k'}{N} \frac{q}{M}}$. Hence, by making the phase compensation approximation, we obtain the equivalent integer delay tap model as

$$\begin{aligned} \hat{y}^{(l')}_{k'} &\approx \sum_{p=0}^{P-1} \sum_{i=-N_g}^{N_g} \sum_{q=-N_d}^{N_d} \hat{h}'_p[q, i] e^{-j2\pi \frac{k'q}{MN}} \hat{x}[l' - q, k' - i] \\ &= \sum_{i=-N_g}^{N_g} \sum_{q=-N_d}^{N_d} \hat{h}[q, i] e^{-j2\pi \frac{k'q}{MN}} \hat{x}[l' - q, k' - i] \end{aligned} \tag{43}$$

where $\hat{h}[q, i] := \sum_{p=0}^{P-1} \hat{h}'_p[q, i]$, and $N_d = S_d + \max_p \lfloor l_p \rfloor$.

Hence for large values of M, a non-integer delay channel for the DD-OFDM baseband channel is closely approximated by an integer delay channel with more *effective paths*. The error in the phase compensation vanishes by increasing the value of M or equivalently bandwidth. These effective paths

are all that can be measured, in practice, at the system sample rate, since it is only possible to measure the energy in each bin (tap), giving an effective integer-delay channel model with a larger number of paths.

B. CHANNEL ESTIMATION ERROR

To compare the channel estimation error, we consider numerical simulation for the 3GPP EVA model [26] with same parameters as in section VIII-B. However, the path delays are now real valued numbers, and not rounded to integers. We choose the number of significant delay taps per path (*i.e.* the number of effective paths), to be $S_d = 20$.

In Fig. 10, we present the channel estimation error of our channel estimation scheme, for DD-OFDM and OTFS, for a channel with both fractional delay and fractional Doppler, for a UE speed of $v = 200$ kmph, or equivalently a maximum Doppler spread of 0.74 kHz. As can be seen, DD-OFDM outperforms OTFS, as it did in the integer delay case in Fig. 9. The difference in performance compared to the integer-delay case is because the energy from each path is now spread over multiple bins in the DD grid, which means the channel is less sparse, reducing the performance of the channel estimator.

In Fig. 11, we present the channel estimation results for a higher UE speed of $v = 500$ kmph, or equivalently a maximum Doppler spread of 1.85 kHz. As can be seen, OTFS-FCP channel estimation has a slightly higher error floor at this higher speed, while the DD-OFDM estimation performance has not changed significantly, even though the Doppler has more than doubled.

X. SYMBOL ERROR RATE AND SPECTRAL EFFICIENCY

In this section, we compare the Symbol Error Rate (SER) and spectral efficiency performance of OTFS and DD-OFDM using numerical simulations.

The path delays and gains of the channel are realized according to the power delay profile specified in the Extended Vehicular A (EVA) model [26]. See Table 1. For each path p, the Doppler shift $\nu_p = f_c \frac{v}{c} \cos(\theta_p)$ is realized according to Jakes formula, where θ_p is uniformly randomly chosen between $-\pi$ and π. Here, v is the speed of the UE, $f_c = 4$ GHz is the carrier frequency and c is the speed of light. We consider two UE speeds v of 200 kmph and 500 kmph, which correspond to a maximum Doppler shift of 0.74 kHz and 1.85 kHz respectively. We note the considered channel model is a general non-integer delay and non-integer Doppler model. We consider 4 QAM alphabet for the data symbols. The rest of the parameters are given in Table 2.

We consider three schemes, namely DD-OFDM, OTFS with reduced cylic prefix (OTFS-RCP) and OTFS-FCP. For DD-OFDM, the number of cyclic micro-subcarriers (*i.e.* $2N_g$) is taken to be 18 for 200 kmph and 26 for 500 kmph for DD-OFDM. The cyclic prefix symbols for OTFS and DD-OFDM are $N_d, M_{cp} = 16$.

We adopt the Message Passing (MP) algorithm of [5] to perform equalization/detection. The delay-Doppler channel tap measurements are obtained by a pilot at $(l, k) = (M/2, N/2)$ for each scheme. For the MP algorithm, only the taps that are not smaller than 30 dB of the strongest tap are considered for equalization in order to exploit sparsity. The presented results are obtained by averaging over 5×10^3 channel realizations.

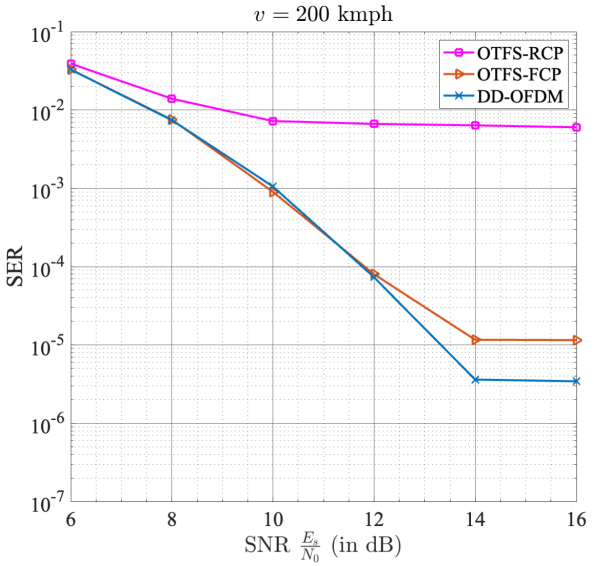

(a) SER curves for $v = 200$ kmph which corresponds to a maximum Doppler spread of 0.74 kHz.

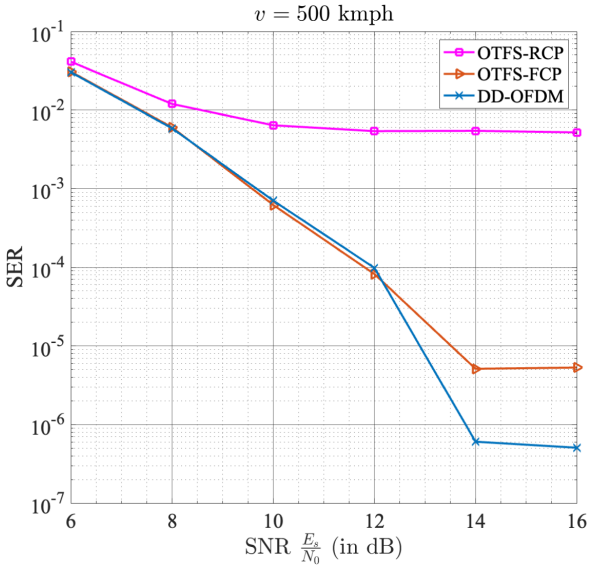

(b) SER curves for $v = 500$ kmph which corresponds to a maximum Doppler spread of 1.85 kHz.

FIGURE 12. SER comparison of OTFS and DD-OFDM for $v = 200$ kmph and $v = 500$ kmph.

TABLE 1. Power delay profile for extended vehicular a model.

Path p	1	2	3	4	5
Delay τ_p (in μs)	0	0.03	0.15	0.31	0.37
Relative Gain (in dB)	0	−1.5	−1.4	−3.6	−0.6

Path p	6	7	8	9
Delay τ_p (in μs)	0.71	1.09	1.73	2.5
Relative Gain (in dB)	−9.1	−7	−12	−16.9

TABLE 2. Simulation parameters.

Parameter	Value
DD grid dimensions (M, N)	$(250, 50)$
Carrier frequency f_c	4 GHz
Bandwidth $M\Delta f$	3.75 MHz
Data modulation alphabet	4 QAM
UE speeds	200 kmph & 500 kmph

TABLE 3. Spectral efficiencies.

Scheme	Spectral Efficiency
OTFS-RCP	$\frac{MN}{MN+N_d} \approx 99.9\%$
DD-OFDM	$\frac{MN}{MN+N_d+2N_g} \approx 99.7\%$
OTFS-FCP	$\frac{(M-N_d)N}{MN} \approx 93.6\%$

A. SER COMPARISON

Fig. 12 presents the curves for SER vs Signal-to-Noise Ratio (SNR) per symbol, $\frac{E_s}{N_0}$. Observe that at both UE speeds DD-OFDM has the lowest SER of the three schemes. The error floor occurs due to the error made from estimating the effective channel matrix from the measured channel taps. As shown in Fig. 10, DD-OFDM has a smaller channel estimation error, which has translated into a superior SER performance over OTFS.

It can also be noted that the SERs of all schemes are lower at the higher UE speed (500 kmph, compared to 200 kmph), which is due to the better separation of paths in the DD domain at higher UE speed.

B. SPECTRAL EFFICIENCY COMPARISON

The spectral efficiencies of the four schemes are given in Table 3, calculated as the ratio of number of data symbols and the time bandwidth product of each waveform (accounting for the cyclic prefix, subcarrier cyclic symbols and bandwidth expansion).

Note that even though OTFS-RCP has a slightly higher spectral efficiency than DD-OFDM, we have seen in Section X-A that it clearly has a significantly worse SER performance.

XI. CONCLUSION

We have presented a new DD modulation scheme, DD-OFDM, by taking an alternate view of ICI and coherence time for an OFDM system in doubly dispersive channels. We have developed DD-OFDM modulation using an OFDM system with micro-subcarriers and DD domain precoding. We have shown that DD-OFDM offers several advantages over OTFS in terms of lower out-of-band emissions, lower SER and better spectral efficiency while having the same sparse channel benefits, PAPR, and comparable implementation complexity.

We have derived the I/O twisted convolution relationship for DD-OFDM, where the phase compensation term only depends on the path delays. As a result, we have proposed a simple channel estimation scheme for DD-OFDM and OTFS in non-integer fractional Doppler channels, and shown that the DD-OFDM performance is superior.

APPENDIX A
PROOFS

Proof of Theorem 1:

$$\int_0^{NT} \zeta_k^{(l)}(t)\zeta_{k'}^{*(l')}(t)dt$$

$$= \frac{1}{M^2NT}\int_0^{NT} e^{j2\pi(k-k')\frac{\Delta f}{N}t}\sum_{m=0}^{M-1} e^{-j2\pi m\left(\frac{l}{M}-\Delta ft\right)} \sum_{m'=0}^{M-1} e^{j2\pi m'\left(\frac{l'}{M}-\Delta ft\right)}dt \tag{44}$$

$$= \frac{1}{M^2}\sum_{m=0}^{M-1}\sum_{m'=0}^{M-1} e^{j2\pi\frac{m'l'-ml}{M}} e^{-j\pi(mN+k-m'N-k')} \operatorname{sinc}\left(mN+k-m'N-k'\right) \tag{45}$$

$$= \frac{1}{M^2}\sum_{m=0}^{M-1} e^{-j2\pi\frac{m(l-l')}{M}}\delta[k-k'] \tag{46}$$

where (46) is due to the fact that $\operatorname{sinc}(\cdot)$ is zero for all integers except 0. From (7), the definition of $\mathcal{F}_M(\cdot)$, we obtain that (46) is equivalent to $\int_0^{NT}\zeta_k^{(l)}(t)\zeta_{k'}^{*(l')}(t)dt = \frac{1}{M}\delta[k-k']\mathcal{F}_M(l-l')$. Since $\mathcal{F}_M(0) = 1$, and $\mathcal{F}_M(m) = 0$ for all integers $m \neq 0$ in the range $\{-M-1,\ldots,M-1\}$, we obtain $\int_0^{NT}\zeta_k^{(l)}(t)\zeta_{k'}^{*(l')}(t)dt = \frac{1}{M}\delta[k-k']\delta[l-l']$. □

Proof of Theorem 2: From (6), the DD-OFDM waveform $x(t)$ can be expressed as

$$x(t) = \frac{1}{\sqrt{MNT}}\sum_{m=0}^{M-1}\sum_{k=0}^{N-1}\tilde{x}_k^{(m)}e^{j2\pi(mN+k)\frac{\Delta f}{N}t}\mathbb{I}_{(0,NT]}. \tag{47}$$

Hence, $X(f)$ can be obtained as

$$X(f) = \frac{1}{\sqrt{M}}\sum_{m=0}^{M-1}\sum_{k=0}^{N-1}\tilde{x}_k^{(m)}\operatorname{sinc}\left(\frac{f}{\Delta f/N}-(mN+k)\right) e^{-j\pi\left(\frac{f}{\Delta f/N}-(mN+k)\right)}. \tag{48}$$

Note that $\mathbb{E}[\tilde{x}_k^{(m)}\tilde{x}_{k'}^{*(m')}] = \delta[m-m']\delta[k-k']$ since $\tilde{x}_k^{(m)}$'s are obtained by taking a DFT of $\hat{x}_k^{(l)}$ along l, where $\hat{x}_k^{(l)}$ are i.i.d such that $\mathbb{E}[\hat{x}_k^{(l)}] = 0$, and $\mathbb{E}[|\hat{x}_k^{(l)}|^2] = \mathbb{E}[\hat{x}_k^{(l)}\hat{x}_k^{*(l)}] = 1$. Hence, we obtain the expected power spectral density for DD-OFDM transmitted signal as

$$\mathbb{E}[|X(f)|^2] = \frac{1}{M}\sum_{m=0}^{M-1}\sum_{k=0}^{N-1}\operatorname{sinc}^2\left(\frac{f}{\Delta f/N}-(mN+k)\right) \tag{49}$$

For OTFS, note that the transmitted signal can be expressed using time-frequency symbols $X_n^{(m)} := \sum_{l=0}^{M-1}\sum_{k=0}^{N-1}\hat{x}_k^{(l)} e^{j2\pi\left(\frac{ml-nk}{MN}\right)}$ as

$$x_{\text{otfs}}(t) = \frac{1}{\sqrt{MNT}}\sum_{m=0}^{M-1}\sum_{n=0}^{N-1}X_n^{(m)}e^{j2\pi m\Delta ft}\mathbb{I}_{[nT,(n+1)T)} \tag{50}$$

Hence, the Fourier transform $X(f)$ can be obtained as

$$X_{\text{otfs}}(f) = \frac{1}{\sqrt{M}} \sum_{m=0}^{M-1} \frac{1}{N} \sum_{n=0}^{N-1} X_n^{(m)} \text{sinc}\left(\frac{f}{\Delta f} - m\right) e^{-j\pi(2n+1)\left(\frac{f}{\Delta f} - m\right)} \quad (51)$$

Note that $\mathbb{E}[X_n^{(m)} X_{n'}^{*(m')}] = \delta[m-m']\delta[n-n']$ as before, since $X_n^{(m)}$'s are obtained by taking a DFT of $\hat{x}_k^{(l)}$ along k and an IDFT along l. Hence, we obtain the expected power spectral density for OTFS transmitted signal as

$$\mathbb{E}[|X_{\text{otfs}}(f)|^2] = \frac{1}{M} \sum_{m=0}^{M-1} \frac{1}{N} \sum_{n=0}^{N-1} \text{sinc}^2\left(\frac{f}{\Delta f} - m\right) \quad (52)$$

$$= \frac{1}{M} \sum_{m=0}^{M-1} \text{sinc}^2\left(\frac{f}{\Delta f} - m\right) \quad (53)$$

□

Proof of Theorem 3: Consider (25). As mentioned, we are only interested in the values of s for which the sinc function value is significant, *i.e.* s such that $|s - mN + k' - \lfloor k_p \rfloor| \leq S$. Note that $|s - mN + k' - \lfloor k_p \rfloor| \leq S$ only if $s \geq mN + (k' - \lfloor k_p \rfloor - S)$ and $s \leq mN + k' - \lfloor k_p \rfloor + S$, which is true only if $s \in \{mN + (k' - N_g), \ldots, mN + (k' + N_g)\}$, since $N_g = S + \max_p \lfloor k_p \rfloor$. Hence, we can write (25) as

$$\tilde{y}_{mN+k'} := \sum_{p=0}^{P-1} \sum_{s=mN+k'-N_g}^{mN+k'+N_g} h'_p e^{-j2\pi s \frac{\Delta f}{N} \tau_p} \tilde{x}_s \, e^{j\pi(s-mN-k'+k_p)} \text{sinc}\left(s - (mN + k' - k_p)\right) \quad (54)$$

Following similarly as in the integer case, we obtain

$$\tilde{y}_{k'}^{(m)} := \sum_{p=0}^{P-1} \sum_{i=-N_g}^{N_g} h'_p e^{-j2\pi(mN+k'-i)\frac{l_p}{MN}} e^{j\pi(k_p-i)} \text{sinc}(k_p - i)\tilde{x}[m, k'-i] \quad (55)$$

As before, we use (22) and (4) to obtain the DD domain baseband equations as

$$\hat{y}_{k'}^{(l')} = \sum_{p=0}^{P-1} \sum_{i=-N_g}^{N_g} \hat{h}_p[i] e^{-j2\pi \frac{k' l_p}{MN}} \mathcal{F}_M\left(l_p - l' + l\right) \hat{x}[l, k'-i]$$

$$= \sum_{p=0}^{P-1} \sum_{i=-N_g}^{N_g} \hat{h}_p[i] e^{-j2\pi \frac{k' l_p}{MN}} \hat{x}[(l'-l_p)_M, k'-i] \quad (56)$$

where $\hat{h}_p[i] := h'_p e^{j\pi(k_p-i)} e^{j2\pi \frac{il_p}{MN}} \text{sinc}(k_p - i)$.

□

APPENDIX B
ON THE USE OF CYCLIC SYMBOLS IN SUBCARRIER DOMAIN

As mentioned previously in footnote 4 of Section VII, it is not essential to fill additional micro-subcarriers on either side of the bandwidth with cyclic symbols. If those micro-subcarriers are left unused, it is analogous to using zeros in the time-domain prefix of traditional OFDM, as is sometimes employed in practice. In this case, all the DD-OFDM baseband equations (*i.e.* (30), Theorem 3 and (41)-(43)) in the paper still hold, provided the definition of $\tilde{x}[m, k]$ in (28) is modified to be

$$\tilde{x}[m,k] := \begin{cases} \tilde{x}_k^{(m)} & \text{if } k \in [0, N-1], m \in [0, M-1] \\ \tilde{x}_{(k)_N}^{(m-1)} & \text{if } k < 0 \ \& \ m > 0 \\ \tilde{x}_{(k)_N}^{(m+1)} & \text{if } k > N-1 \ \& \ m < M-1 \\ 0 & \text{o.w.} \end{cases} \quad (57)$$

and as a result, $\hat{x}[l, k]$ from (29) is replaced by:

$$\hat{x}[l,k] := \begin{cases} \hat{x}_k^{(l)} & \text{if } k \in [0, N-1] \\ \left(1 - \frac{1}{N}\right) e^{j2\pi \frac{l}{M}} \hat{x}_{(k)_N}^{(l)} & \text{if } k < 0 \\ \left(1 - \frac{1}{N}\right) e^{-j2\pi \frac{l}{M}} \hat{x}_{(k)_N}^{(l)} & \text{if } k > N-1 \end{cases} \quad (58)$$

REFERENCES

[1] S. K. Mohammed, "Derivation of OTFS modulation from first principles," *IEEE Trans. Veh. Technol.*, vol. 70, no. 8, pp. 7619–7636, Aug. 2021.

[2] R. Hadani, S. Rakib, M. Tsatsanis, A. Monk, A. J. Goldsmith, A. F. Molisch, and R. Calderbank, "Orthogonal time frequency space modulation," in *Proc. IEEE Wireless Commun. Netw. Conf. (WCNC)*, Mar. 2017, pp. 1–6.

[3] R. Hadani and A. Monk, "OTFS: A new generation of modulation addressing the challenges of 5G," 2018, *arXiv:1802.02623*.

[4] P. Raviteja, K. T. Phan, Y. Hong, and E. Viterbo, "Interference cancellation and iterative detection for orthogonal time frequency space modulation," *IEEE Trans. Wireless Commun.*, vol. 17, no. 10, pp. 6501–6515, Oct. 2018.

[5] P. Raviteja, K. T. Phan, and Y. Hong, "Embedded pilot-aided channel estimation for OTFS in delay–Doppler channels," *IEEE Trans. Veh. Technol.*, vol. 68, no. 5, pp. 4906–4917, May 2019.

[6] S. K. Mohammed, "Time-domain to delay-Doppler domain conversion of OTFS signals in very high mobility scenarios," *IEEE Trans. Veh. Technol.*, vol. 70, no. 6, pp. 6178–6183, Jun. 2021.

[7] G. Matz, H. Bolcskei, and F. Hlawatsch, "Time-frequency foundations of communications: Concepts and tools," *IEEE Signal Process. Mag.*, vol. 30, no. 6, pp. 87–96, Nov. 2013.

[8] W. Kozek and A. F. Molisch, "Nonorthogonal pulseshapes for multicarrier communications in doubly dispersive channels," *IEEE J. Sel. Areas Commun.*, vol. 16, no. 8, pp. 1579–1589, Jun. 1998.

[9] K. Liu, T. Kadous, and A. M. Sayeed, "Orthogonal time–frequency signaling over doubly dispersive channels," *IEEE Trans. Inf. Theory*, vol. 50, no. 11, pp. 2583–2603, Nov. 2004.

[10] S. Das and P. Schniter, "Max-SINR ISI/ICI-shaping multicarrier communication over the doubly dispersive channel," *IEEE Trans. Signal Process.*, vol. 55, no. 12, pp. 5782–5795, Dec. 2007.

[11] P. Raviteja, Y. Hong, E. Viterbo, and E. Biglieri, "Practical pulse-shaping waveforms for reduced-cyclic-prefix OTFS," *IEEE Trans. Veh. Technol.*, vol. 68, no. 1, pp. 957–961, Jan. 2019.

[12] H. Qu, G. Liu, L. Zhang, S. Wen, and M. A. Imran, "Low-complexity symbol detection and interference cancellation for OTFS system," *IEEE Trans. Commun.*, vol. 69, no. 3, pp. 1524–1537, Mar. 2021.

[13] M. Kollengode Ramachandran and A. Chockalingam, "MIMO-OTFS in high-Doppler fading channels: Signal detection and channel estimation," in *Proc. IEEE Global Commun. Conf. (GLOBECOM)*, Dec. 2018, pp. 206–212.

[14] A. Naikoti and A. Chockalingam, "Signal detection and channel estimation in OTFS," *ZTE Commun.*, vol. 19, no. 4, pp. 16–33, Dec. 2021.

[15] C. Jin, Z. Bie, X. Lin, W. Xu, and H. Gao, "A simple two-stage equalizer for OTFS with rectangular windows," *IEEE Commun. Lett.*, vol. 25, no. 4, pp. 1158–1162, Apr. 2021.
[16] T. Thaj, E. Viterbo, and Y. Hong, "General I/O relations and low-complexity universal MRC detection for all OTFS variants," *IEEE Access*, vol. 10, pp. 96026–96037, 2022.
[17] A. Farhang, A. RezazadehReyhani, L. E. Doyle, and B. Farhang-Boroujeny, "Low complexity modem structure for OFDM-based orthogonal time frequency space modulation," *IEEE Wireless Commun. Lett.*, vol. 7, no. 3, pp. 344–347, Jun. 2018.
[18] V. Rangamgari, S. Tiwari, S. S. Das, and S. C. Mondal, "OTFS: Interleaved OFDM with block CP," in *Proc. Nat. Conf. Commun. (NCC)*, Feb. 2020, pp. 1–6.
[19] N. Hashimoto, N. Osawa, K. Yamazaki, and S. Ibi, "Channel estimation and equalization for CP-OFDM-based OTFS in fractional Doppler channels," in *Proc. IEEE Int. Conf. Commun. Workshops (ICC Workshops)*, Jun. 2021, pp. 1–7.
[20] L. Zhao, W.-J. Gao, and W. Guo, "Sparse Bayesian learning of delay-Doppler channel for OTFS system," *IEEE Commun. Lett.*, vol. 24, no. 12, pp. 2766–2769, Dec. 2020.
[21] F. Liu, Z. Yuan, Q. Guo, Z. Wang, and P. Sun, "Message passing-based structured sparse signal recovery for estimation of OTFS channels with fractional Doppler shifts," *IEEE Trans. Wireless Commun.*, vol. 20, no. 12, pp. 7773–7785, Dec. 2021.
[22] D. Shi, W. Wang, L. You, X. Song, Y. Hong, X. Gao, and G. Fettweis, "Deterministic pilot design and channel estimation for downlink massive MIMO-OTFS systems in presence of the fractional Doppler," *IEEE Trans. Wireless Commun.*, vol. 20, no. 11, pp. 7151–7165, Nov. 2021.
[23] S. S. Das, V. Rangamgari, S. Tiwari, and S. C. Mondal, "Time domain channel estimation and equalization of CP-OTFS under multiple fractional dopplers and residual synchronization errors," *IEEE Access*, vol. 9, pp. 10561–10576, 2021.
[24] Y. Yamashita and H. Ochiai, "Performance comparison of coded OFDM with DFT-precoding over nonlinear channels," in *Proc. IEEE Int. Conf. Ubiquitous Wireless Broadband (ICUWB)*, Oct. 2015, pp. 1–5.
[25] T. Dean, M. Chowdhury, and A. Goldsmith, "A new modulation technique for Doppler compensation in frequency-dispersive channels," in *Proc. IEEE 28th Annu. Int. Symp. Pers., Indoor, Mobile Radio Commun. (PIMRC)*, Oct. 2017, pp. 1–7.
[26] 3GPP, "Evolved universal terrestrial radio access (E-UTRA); base station (BS) radio transmission and reception," Tech. Specification (TS) 36.104, 3rd Generation Partnership Project (3GPP), Version 18.2.0, Jun. 2023.

SWAROOP GOPALAM (Member, IEEE) received the B.Tech. degree in electrical engineering from Indian Institute of Technology (IIT) Bombay, in 2014, and the M.Res. and Ph.D. degrees in engineering from Macquarie University, Sydney, NSW, Australia, in 2017 and 2021 respectively.

Since 2021, he has been a Research Fellow with the School of Engineering, Macquarie University. His research interests include delay-Doppler domain communication, resource allocation in wireless networks, and the design of distributed and low-complexity algorithms.

SIBIRAJ B. PILLAI received the Ph.D. degree in computer science and communication systems from École Polytechnique Fédérale de Lausanne (EPFL), Switzerland, in July 2007. From October 2007 to April 2009, he was a Research Fellow with the University of Melbourne. Since then, he has been a Faculty Member with the Department of Electrical Engineering, Indian Institute of Technology Bombay. His research interests include network information theory, feedback communications, cross-layer scheduling, biological information inheritance, and radar signal processing.

PHILIP WHITING received the B.A. degree from the University of Oxford, the M.Sc. degree from the University of London, U.K., and the Ph.D. degree in queueing theory from the University of Strathclyde. After a postdoctoral position with the University of Cambridge, his research interest includes wireless. In 1993, he participated in the Telstra Trial of Qualcomm CDMA in South Eastern Australia. Then, he joined the Mobile Research Centre, University of South Australia, Adelaide, Australia. From January 1997 to June 2013, he was a Researcher with Bell Labs. Since July 2013, he has been with Macquarie University, Sydney, NSW, Australia, where he is currently a Research Fellow. His main research interests include the mathematics of wireless networks, stochastic models for resource allocation, statistics for large-scale data, mm wave wireless networks, CSMA networks, and load balancing for cloud computing and HetNets.

HAZER INALTEKIN (Member, IEEE) received the B.S. degree (Hons.) in electrical and electronics engineering from Boğaziçi University, Istanbul, Turkey, and the M.S./Ph.D. degree in electrical and computer engineering from Cornell University, Ithaca, NY, USA. He is currently a Senior Lecturer with Macquarie University. Prior to joining Macquarie University, he held various researcher and faculty positions in Australia, Europe, and USA. His research interests include airborne networks, satellite communications, fog/edge computing, the IoT, wireless communications, and information theory.

IAIN B. COLLINGS (Fellow, IEEE) received the Ph.D. degree in systems engineering from The Australian National University, in 1995. He is currently a Professor with the School of Engineering, Macquarie University, Sydney, NSW, Australia. Previously, he spent nine years at the CSIRO, where he held a number of roles, including the Deputy Chief of Division, the Research Program Leader, and the Theme Leader, and nine years with the Universities of Melbourne and Sydney. He has published more than 300 papers in the area of wireless communications. He was awarded the Engineers Australia IREE Neville Thiele Award, in 2009, and the IEEE CommSoc Stephen O. Rice Award, in 2011. He served as an Editor for IEEE TRANSACTIONS ON WIRELESS COMMUNICATIONS.

STEPHEN V. HANLY (Fellow, IEEE) received the Ph.D. degree in mathematics from Cambridge University, U.K., in 1994. He is currently a Professor with the School of Engineering, Macquarie University, Sydney, NSW, Australia. His research interest includes wireless communications. He was a recipient of the INFOCOM Best Paper Award, the IEEE Information Theory Society, the IEEE Communication Society Joint Paper Award, and the IEEE Communications Society Tutorial Paper Award. He has been an Associate Editor of IEEE TRANSACTIONS ON WIRELESS COMMUNICATIONS and a Guest Editor of the IEEE JOURNAL ON SELECTED AREAS IN COMMUNICATIONS. He has taken major roles at several IEEE conferences and workshops, including IEEE ISIT and IEEE CTW.